Fluoride-induced interfacial adhesion loss of nanoporous anodic aluminum oxide templates in aerospace structures

Abrahami, Shoshan; de Kok, John; Gudla, V.C.; Marcoen, Kristof; Hauffman, T.; Ambat, R.; Mol, Arjan; Terryn, Herman

Important note
To cite this publication, please use the final published version (if applicable).
Please check the document version above.

Fluoride-Induced Interfacial Adhesion Loss of Nanoporous Anodic Aluminum Oxide Templates in Aerospace Structures

S. T. Abrahami,[†,‡,§] J. M. M. de Kok,[∥] V. C. Gudla,[⊥] K. Marcoen,[§] T. Hauffman,[§] R. Ambat,[⊥] J. M. C. Mol,[†]● and H. Terryn*[,†,§]●

[†]Department of Materials Science and Engineering, Delft University of Technology, Mekelweg 2, 2628 CD Delft, The Netherlands

[‡]Materials innovation institute, Van der Burghweg 1, 2628 CS Delft, The Netherlands

[§]Department of Materials and Chemistry, Research Group Electrochemical and Surface Engineering, Vrije Universiteit Brussel, Pleinlaan 2, 1050 Brussels, Belgium

[∥]Fokker Aerostructures BV, Industrieweg 4, 3351 LB Papendrecht, The Netherlands

[⊥]Section of Materials and Surface Engineering, Department of Mechanical Engineering, Technical University of Denmark, Produktionstorvet, Kongens Lyngby 2800, Denmark

Ⓢ *Supporting Information*

ABSTRACT: Nanoporous anodic aluminum oxides (AAOs) are used as templates in various technological applications, including load-bearing aircraft structures. But in spite of their popularity, the important aspects that control their (dis-)bonding to an organic coating are not fully understood. To study the mechanisms behind the negative effect of fluorides on AAOs adhesion we employed both porous and barrier AAO specimens. These were prepared by anodizing in sulfuric acid (SAA) or a mixture of phosphoric and sulfuric acids (PSA), with and without postanodizing immersion in NaF. Experimental results indicate that chemical surface modifications, as concluded from X-ray photoelectron spectroscopy and time-of-flight secondary ion mass spectrometry, are dependent on the initial oxide composition. A partial replacement of surface hydroxyls (OH) by fluorine on SAA leads to adhesion loss due to removal of these stable sites for oxide-to-adhesive interfacial bonding. Conversely, fluoride-induced dissolution of surface phosphates in PSA compensates for fluoride adsorption by revealing new OH groups. As the net OH fraction remains similar there is no further adhesion loss under water-ingress. The surprising reduction of dry adhesion is contributed to an interplay between surface energy changes affecting the type of attractive forces across the interface, as well as the loss of fine surface features, as seen by transmission electron microscopy cross-section images.

KEYWORDS: aluminum, anodizing, adhesion, fluorides, nanotemplates
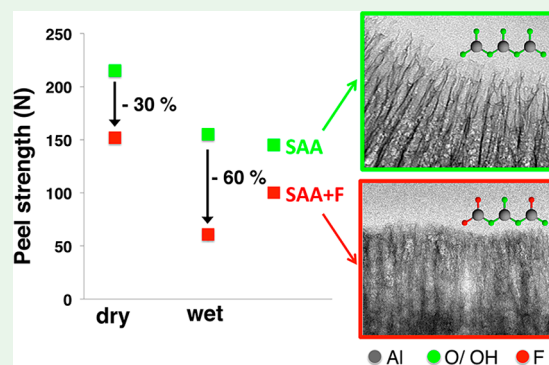
INTRODUCTION

Anodizing of is one of the most prominent industrial surface treatments used to produce durable protective anodic aluminum oxide (AAO) films with many desirable engineering properties such as corrosion and wear resistance. Anodizing can produce both barrier and porous layers, but porous oxides are by far more industrially important, as their porosity serves as an excellent base for further surface finishing such as sealing, painting, adhesion, electroplating, or certain decorative functions.[1] Such anodized products can be found in packaging, architecture, electronics, lithography, or automotive and aerospace components. In recent years anodizing has also become one of the simplest available commercial methods to produce templates for the fabrication of nanostructured materials.[2] By controlling the process parameters such as the electrolyte properties (composition, concentrations) and the anodizing conditions (voltage, time, temperature) this process enables the production of nanotemplates with a wide range of dimensions. Advances in nanotechnology have further driven the development of countless specialized procedures to produce AAO nanotemplates with complex geometries for specialized technological applications such as sensors, catalysis, molecular membranes, MEMS, and biomedical devices.[3,4]

But despite their popularity, the important aspects that control (dis-) bonding between the AAO templates and organic coatings are not fully understood. While some of the previously mentioned applications require a strong and durable interfacial bonding between the two phases, others will benefit from a more inert nature of the AAO mold. In the absence of additional treatments, the interfacial properties of porous AAOs are inherent to the chosen electrolyte and final morphology. The most crucial aspect that determines the structure and interfacial

properties of these porous AAOs is the surface pretreatment.[5] The first step in this process is cleaning the aluminum surface from external contaminations such as grease and inks. Hereafter, the top few microns of the surface material are etched to remove surface layers from manufacturing induced damage and near-surface artifacts.[6] Anodizing in an acid electrolyte generally follows this step, resulting in a duplex nanoporous oxide layer.

This array of pretreatment steps is generally based on aqueous solutions that often contain different additives for acceleration of surface reactions and bath stabilization. Historically in the aerospace industry, chromic acid was the main ingredient in most etching solutions.[7] However, in the attempt to avoid this toxic substance, many wet etching solutions now contain fluorides, as these have been used for more than a decade for the activation of aluminum (and other metals) in the production of chemical conversion layers.[8] The presence of F^- ions enables metal activation by dissolution and replacement of certain O^{2-} lattice anions[9] or by forming surface complexes.[10] The mechanism of chemical dissolution consists of the formation of an Al−F complex by adsorption of the free fluorides, which later desorb from the surface toward the bulk solution. From all metals studied by Cerezo et al.,[11] the influence of surface hydroxyls on the formation of the conversion coating was most dominant for aluminum, and the dissolution in this case was solely attributed to fluoride interaction with surface hydroxyls.

Several publications have even considered adding fluorides to the anodizing bath of aluminum and aluminum alloys.[12−15] They report a beneficial increase in the film growth rate at low to moderate fluoride concentrations. At higher concentrations, chemical dissolution was dominant and affected the film morphological features. The resulting anodic oxides contained incorporated fluorides through the entire film, as the F^- ion migration rate under the influence of the electric field is approximately double the rate of O^{2-} ion migration.[16] So far, these investigations focused on the relation between fluoride additions and the final oxide properties. Yet, aircraft manufacturers have noticed that fluoride contamination in their pretreatment or rinsing baths is detrimental for the subsequent adhesion between the anodized aluminum components.

To our knowledge, the only previous study to mention the effect of fluorides on the adhesion of anodic oxides was completed in 1979 by Venables et al.[17] The authors claimed that fluoride contamination removes the protrusions previously made by sulfuric-chromic acid etching, leaving a thin and flat surface oxide that does not provide mechanical interlocking with the applied organic resin. Yet, in a recent publication we showed that flat oxides can adhere to an epoxy adhesive, with their level of adhesion depending on surface chemistry and the adhesive composition.[18,19] With this new knowledge and with the increasing importance of fluoride ions in Cr(VI)-free surface treatments, this study aims to investigate the fundamental mechanisms behind the loss of adhesion caused by fluorides. Two types of porous anodic aluminum oxide (AAO) structures from our previous work[20] were selected for this case study: a mixture of phosphoric and sulfuric acids (PSA) oxide that exhibits a high level of adhesion and a moderate SAA that could possibly be improved by pore opening. By employing porous and barrier AAO specimens for both chemical characterization and mechanical tests in this study we are able to make a distinction between contributions from morphological and chemical surface modifications.

■ EXPERIMENTAL SECTION

Materials and Sample Preparation. *Barrier AAO.* Specimens for barrier-type anodizing were cut from a 0.3 mm thick sheet of pure aluminum (99.99%, Hydro). To remove the surface imperfections, and to provide a flat substrate suitable for high-resolution surface analysis and quantification, all barrier-type specimens were electropolished in a mixture of 80 vol % ethanol and 20 vol % perchloric acid according to the details described in ref 21. Galvanostatic anodizing was performed with SM120-25 power supply (Delta Elektronika). A three-electrode cell filled with 400 mL of solution was used with two AA1050 aluminum cathodes. SAA specimens were prepared in 10 g/L H_2SO_4 at 0.2 A and 35 °C for 4 s. PSA was prepared in the same conditions, with 40 g/L H_3PO_4 and 10 g/L H_2SO_4. After they were anodized, the substrates were thoroughly rinsed with running demineralized water for 30 s and subsequently ultrasonically rinsed for 3 min. Anodizing conditions were preselected to yield barrier-type anodic oxides by stopping the oxide growth at the end of the region in which the voltage increases linearly with time, which is associated with the formation of a barrier layer.[22] The samples were then cut in half, and one part was immersed in 25 g/L NaF solution for 5 min. The samples were then rinsed with running demineralized water for 30 s and ultrasonically rinsed for an extra 5 min to remove any unbound ions.

Barrier AAOs for floating roller peel testing were prepared from AA2024-T3 alclad (clad layer AA1230) aluminum test panels of 250 × 95 × 1.6 mm and 300 × 95 × 0.5 mm for the thick and thin sheets, respectively. Before anodizing, specimens were degreased, alkaline etched, and desmutted. Degreasing was achieved by wiping the panels with ethanol. This was followed by a 2 min alkaline etching with 40 g/L P3 Almeco 51 (from Henkel) at 35 °C and a 1 min pickling with 35 vol % HNO_3 at room temperature (RT). After each step, the panel was thoroughly rinsed with running demi-water, followed by 1 min immersion rinsing in an agitated beaker of fresh demi-water. Anodization at the same conditions as above, but at 5 mA/cm^2, was performed for 8 s. Although the current density is lower than for the model specimens, the time is doubled, so that the final barrier layer thickness should be similar. After they were anodized, the panels were rinsed and dried with compressed air. The panels were then bonded (without primer) with FM 73 epoxy film adhesive (from Cytec Engineering Materials) within 10 min after the pretreatment of the thin panel was completed. After they were bonded, the panels were stored in a sealed plastic bag for up to 24 h before curing. Curing following the manufacturer instructions was achieved using a Joos hot plate press at 6 bar and 120 °C for 75 min. Sample preparation method and configurations for the different tests are illustrated in Figure 1.

Porous AAO. Industrial porous specimens were prepared from AA2024-clad sheets. Sulfuric acid anodizing (SAA) panels were
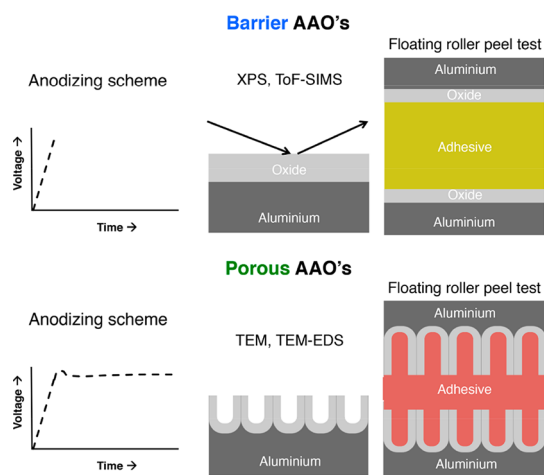
Figure 1. Schematic illustration of the preparation methods, morphologies, and analysis configurations for the two different types of samples that were employed in this study.
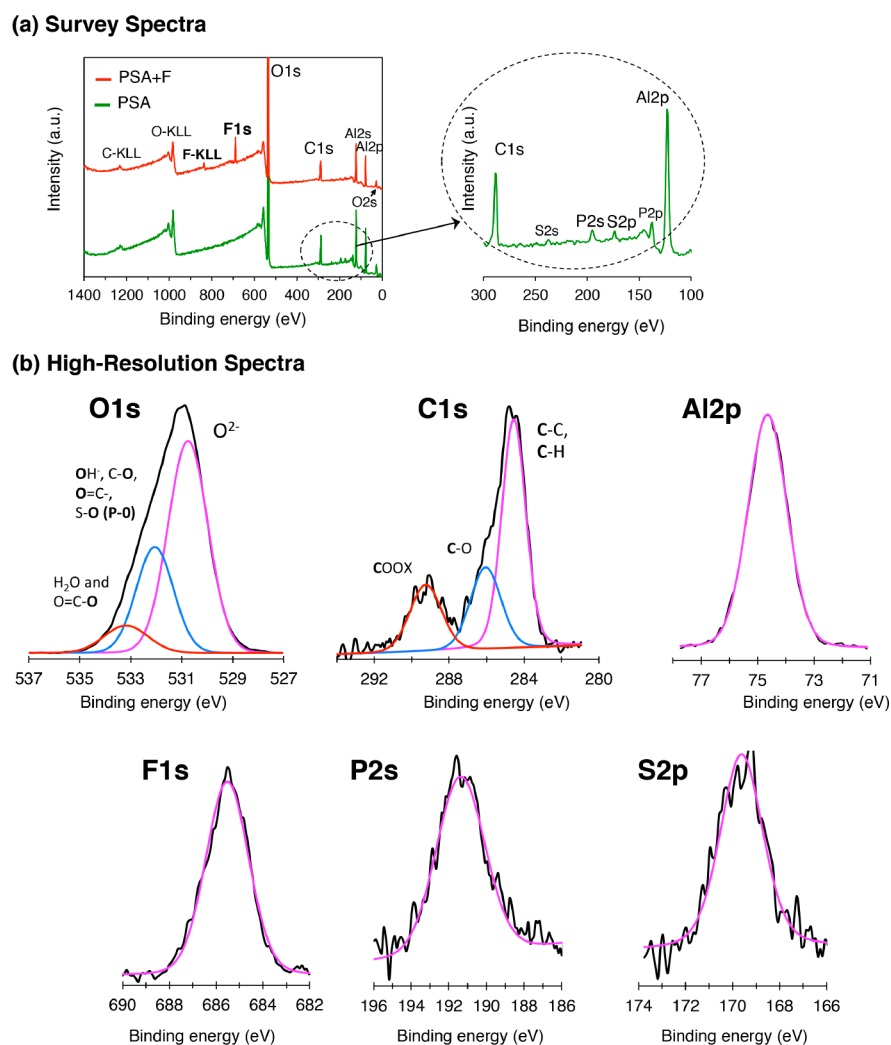
Figure 2. (a) XPS survey spectra for PSA before (green) and after (red) 5 min of immersion in 50 g/L NaF (PSA+F) and (b) example of a high-resolution XPS spectra for O 1s, C 1s, Al 2p, F 1s, P 2s, and S 2p. Fitted peaks for individual species are marked with colored lines, while the measured spectra are shown in black lines. Peak dimensions were scaled for presentation purposes.

anodized in 25 g/L H_2SO_4 for 30 min at 21 V and 35 °C, with 2 g Al^{3+}/L present in the electrolyte. PSA anodizing panels were anodized for 30 min at 28 V and at 35 °C in a mixture of 40 g/L H_3PO_4 and 10 g/L H_2SO_4, also with 2 g Al^{3+}/L. The less-than-optimal SAA conditions (concentration, temperature, and time) were preselected to determine if post-treatment can improve wet adhesion strength, while the PSA conditions were preselected to determine if a high level of performance can be further improved. Both conditions selected from our previous study.[20] Post-treatment was performed in 50 g/L NaF for 5 and 10 min at 25 °C for PSA and SAA, respectively. After treatments, the sheets were applied with phenolformaldehyde primer Redux 101 that was cured at 120 °C. Subsequently they were autoclave-bonded with epoxy adhesive AF 163 at 125C and 6 bar. Porous oxide samples are denoted pSAA, pPSA, pSAA+F, and pPSA+F (in which the p stands for "porous") throughout the paper to differentiate them from barrier samples. It is a matter of importance to note the AF163 adhesive results in higher peel strength values than FM73 adhesive (ca. +10%). Additionally the peel strip with pPSA and pPSA+F was 0.8 mm instead of 0.5 mm, which results in higher peel strength as well (ca. +40%). Sample preparation method and configurations for the different tests are illustrated in Figure 1.

Analysis Methods. *X-ray Photoelectron Analysis (XPS).* XPS spectra were collected using a PHI5600 photoelectron spectrometer (Physical Electronics) with an Al Kα monochromatic X-ray source (1486.71 eV of photons). The vacuum in the analysis chamber was ~5 × 10⁻⁹ Torr during measurements. High-resolution scans of the

Al2p, O1s, C1s, P2s, S2p, and F1s photoelectron peaks were recorded from a spot diameter of 0.8 mm using pass energy of 23.5 eV and step size 0.1 eV. Measurements were performed with a takeoff angles of 15° with respect to the sample surface. Reproducibility of XPS measurements was verified by triplication of the measurements on at least two different specimens (and at a takeoff angle of 45°).

Data were analyzed with PHI Multipak software (V9.5.0.8). Prior to fitting, the energy scale of the XPS spectra was calibrated relative to the binding energy of adventitious hydrocarbons (C−C/C−H, Figure 2e) in the C 1s peak at 284.4 eV. Curve fitting was then done after a Shirley-type background removal, using mixed Gaussian (80−100%)−Lorentzian shapes.

Time-of-Flight Secondary Ion Mass Spectroscopy (ToF-SIMS). ToF-SIMS measurements were performed with a TOF.SIMS⁵ (ION-TOF GmbH). Both positive and negative secondary ion spectra were obtained using a 30 keV Bi_3^+ primary ion beam operated at high current bunched mode with 0.41 pA target current. The total ion dose was kept below the static limit of 1×10^{13} ions cm⁻² analysis⁻¹ on an analysis area of 100 × 100 μm² at 128 × 128 pixels. Three random positions were analyzed on each sample, both in positive and negative mode, to validate that the obtained spectra were reproducible and characteristic for the sample. Reported intensities were normalized using the total ion count. The mass accuracy of a peak assignment or so-called deviation (in ppm) is calculated by dividing the absolute difference between experimental and theoretical mass by the experimental mass.

Table 1. Average Binding Energies ($\pm$ 0.2 eV) from at Least Two Separate XPS Measurements and the Calculated Relative Percentage of Surface Species[a]

	C1s (eV)			O1s (eV)			Al2p (eV)	S2p (eV)	P2s (eV)	F1s (eV)	calcd OH⁻ (%)	calcd SO₄²⁻ (%)	calcd PO₄³⁻ (%)
	1	2	3	1	2	3							
SAA	284.8	286.2	289.3	530.8	532.2	533.2	74.4	169.4			23	3	
SAA+NaF	284.7	286.2	289.2	531.0	532.1	533.2	74.5	169.6		685.2	14	2	
PSA	284.8	286.4	289.4	531.1	532.3	533.5	74.7	169.5	191.6		14	2	4
PSA+NaF	284.8	286.3	289.4	530.8	532.0	533.2	74.3	169.8	191.5	685.6	16	2	2

[a]Subpeak assignments correspond to (1) C−C/C−H, (2) C−O, (3) COOX, (1) O²⁻, (2) OH⁻, C−O, O=C-, and S−O, and (3) H₂O and O=C−O.

Scanning and Transmission Electron Microscopy (SEM and TEM). Cross sections of selected porous-type anodized specimens were cut using a diamond saw and embedded in an epoxy at room temperature. The cross sections were then ground and polished gradually and finished using a 1 μm diamond paste. Lamellas for TEM characterization were then prepared by focused ion beam milling using a Ga liquid-metal ion source and in situ lift out from the interface of the adhesive joint using Helios Nanolab 600 dual beam, FEI coupled to an Omniprobe micromanipulator. The lamellas of ∼1 μm thickness were further thinned for electron transparency to an approximate thickness of 120 nm, and low-energy milling (2 keV) was finally performed to remove any high-energy ion beam milling induced artifacts and damage to the samples.

Focused ion beam (FIB)-prepared lamellas were then transferred to a Tecnai T20 G², FEI for TEM analysis, operating at 200 keV. Bright-field images of the film morphology were recorded for comparison. The local composition of the anodic oxide and the relative concentrations of the resin in the porous structure were also measured using an X-ray energy dispersive spectrometer (EDS, Oxford 80 mm² X-Max SDD detector) coupled to the TEM. Quantification of the obtained EDS data was performed using Aztec TEM EDS software.

Floating Roller Peel Tests. Floating roller peel tests were performed according to ASTM D3167-03a.[23] The bonded panels were cut into 25 mm wide samples using a diamond saw. After the test panels were fixed in the apparatus, the unbounded end of the specimen was attached to the lower head of the testing machine. The thin panel was peeled from the thicker panel with a speed of 100 mm/min. The peeling load versus head movement (or load vs distance peeled) was recorded. All tests were performed at ambient temperature. The first half of the specimen was peeled under dry atmospheric conditions. Water containing surfactant was then applied to the crack-tip, and the second half was peeled under wet conditions.

■ RESULTS AND DISCUSSION

Surface Chemistry of Barrier AAO. Barrier-type oxides were employed to characterize changes in the chemical surface composition using XPS and ToF-SIMS. Figure 2a displays the XPS survey spectra of PSA oxide before and after 5 min of immersion in NaF solution followed by 3 min of rinsing. The main elements in the PSA spectrum in Figure 2a are O, Al, C, P, and S (no P in SAA spectrum). Besides carbon that arises from atmospheric contamination, all other elements observed are inherent to the anodized oxide. The spectrum after immersion in NaF solution (Figure 2a) contains, in addition to the previously mentioned elements, 2−4 atom % of fluorine for both SAA and PSA. No Na was detected in any of the specimens. High-resolution spectra (HRES) of O1s, Al2p, C1s, P2s, S2p, and F 1s were recorded to evaluate changes in the binding states of the surface elements. Examples of the typical HRES photoelectron peaks are shown in Figure 2b from PSA+F surface. The average measured binding energies (BE) are listed in Table 1.

The full-width at half-maximum (fwhm) of the O1s envelope is changing from 2.8 to 2.6 $\pm$ 0.1 eV for SAA and SAA+F,

respectively. The fwhm values of 2.8 and 2.7 $\pm$ 0.1 eV were recorded for PSA and PSA+F, respectively. No changes in the fwhm were recorded for Al2p (1.7 eV). Sulfur and phosphor are found at 169.7 and 191.5 eV, respectively. These binding energies correspond to sulfates and phosphates.[21] The average binding energy of fluorine F1s was 685.3 $\pm$ 0.1 eV with fwhm of 2.2 eV. The binding energy for F in the ionic bond AlF₃ is 687.8 eV with fwhm of 3.0 eV.[24] According to the Eh-pH diagram (HSC Chemistry V6), AlF₃ is also not stable in the alkaline conditions that were applied in this study. The thermodynamically stable species are F⁻ and AlOOH (Figures S1 and S2 in the Supporting Information). Hence, the lower binding energy of fluorine on the SAA and PSA oxides indicates a weaker nature of interaction between the anodic surface and the fluoride ions. To evaluate relative changes in the chemical composition of the surface groups, HRES data was fitted into the subcomponents shown in Figure 2b, following the method described in Abrahami et al.[21] The results are listed in Table 1. Fitting the different groups and calculating the relative amount of surface hydroxyls (while accounting for the contribution of surface contamination) reveal that there is a reduction in the amount of surface hydroxyls on SAA+F oxide compared to SAA (therefore the narrower fwhm of O1s) and minor reduction in the sulfate content. Conversely, PSA+F has a larger amount of surface hydroxyls compared to PSA, as well as a reduced number of phosphates, with no change in the relative amount of sulfates.

Positive and negative ToF-SIMS spectra were acquired to obtain a better understanding of the effect of fluorides on the chemical composition of the different oxides. Selected fragments of interest are shown in Figures 3−5, and a detailed fragment list is given in Table 2. Peaks at nominal masses 96, 79, and 122 m/z were identified as SO₄⁻, PO₃⁻, and AlPO₄⁻, respectively (Figure 3a−c), and they confirm the presence of sulfates and phosphates, in agreement with the previous XPS analysis. Fluorides are found only on PSA+F and SAA+F, as shown by fragments as F⁻, AlOF⁻, and AlOF₂⁻, which are found at nominal masses 19, 62, and 81 m/z, respectively (Figure 3d,e).

Fragments such as AlOF⁻ and AlOF₂⁻ show that fluoride ions interacted with the anodic surface, but they do not clarify whether the fluorides are bonded to oxygen or to aluminum. In a higher mass range, fragments were found that give insights into bonding configurations. Peaks at nominal masses 197, 199, 201, 203, and 205 m/z were identified as Al₃O₇H₄⁻, Al₃O₆H₃F⁻, Al₃O₅H₂F₂⁻, Al₃O₄HF₃⁻, and Al₃O₃F₄⁻, respectively (Figure 4a), and they form a series of fragments in which surface hydroxyl groups are gradually replaced by fluorides. This is illustrated by their proposed chemical structures that were added next to the spectra. Al₃O₇H⁻ is a fragment that can be considered saturated with hydroxyl groups, while Al₃O₃F₄⁻ is a fragment that is fully fluorinated. For ease of reference, fragments will be
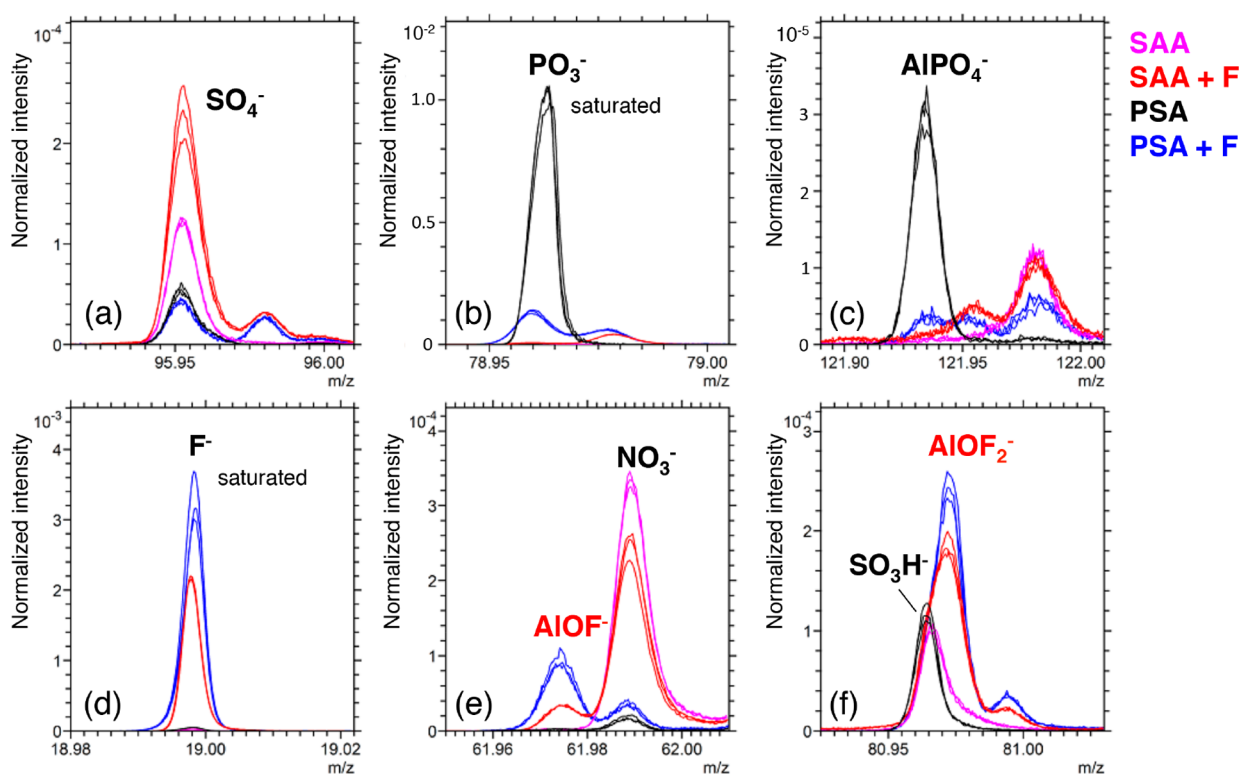
Figure 3. Comparison of the (normalized) measured ToF-SIMS spectra of fragments showing the presence of sulfates and phosphates (a−c) and fluorides (d−f) on the surfaces of the different barrier AAOs (overlay of three spectra per sample).

Table 2. Selected (Negative) ToF-SIMS Fragments Mass, Deviation, and Resolution

| fragment	mass	deviation	resolution
$AlOF^-$	61.9740u	−22 ppm	8992
$AlO_3H_2^-$	76.9834u	11.4 ppm	8696
$AlOF_2^-$	80.9711u	−33 ppm	5806
$AlPO_4^-$	121.9359u	3.5 ppm	9049
$Al_2O_5H_3^-$	136.9631u	10.4 ppm	8228
$Al_3O_7H_4^-$	196.9413u	2 ppm	8468
$Al_3O_6H_3F^-$	198.9358u	−3 ppm	7996
$Al_3O_5H_2F_2^-$	200.9319u	−1 ppm	8378
$Al_3O_4HF_3^-$	202.9272u	−3 ppm	8586
$Al_3O_3F_4^-$	204.9227u	−4 ppm	8380

denoted as 0F, 1F, 2F, 3F, and 4F, depending on the number of fluorides they contain. Figure 4b shows a bar graph in which normalized peak areas are plotted for fragments 0F to 4F. On the one hand, for SAA, only 0F was found in its mass spectrum, with a normalized intensity more than double the intensity found for 0F in SAA+F. On the other hand, the intensity distribution in SAA+F shows a maximum for fragment 1F, directly followed by 2F. As such, the observations presented in Figure 4 clearly demonstrate the partial replacement of surface hydroxyls by fluorides on SAA+F, in which fluorides bond directly with aluminum. The general trend is different for PSA and PSA+F. The dominance of fragments 1F, 2F, and 3F in the spectrum of PSA+F shows that, in a similar manner to SAA+F, fluorides bond directly with aluminum. However, relative to PSA, the normalized intensity of hydroxyl fragment 0F is significantly higher for PSA+F. This is in accordance with the previous XPS results and demonstrates that fluoride adsorption

on PSA+F did not occur through replacement of surface hydroxyl groups.

It was further investigated whether ToF-SIMS results support XPS analysis regarding surface hydroxyl fractions. A peak at nominal mass 44 m/z, identified as $AlOH^+$ (Figure 5b), could be expected to reflect the variations in hydroxyl fraction among the different oxides. However, in contrast to the XPS results, significantly higher intensities are found for PSA+F, compared to all other oxides. Furthermore, peak intensities of fragments such as Al^+ (Figure 5a), AlO^+ (not shown), and AlO_2^- (Figure 5c) are also significantly higher for PSA+F. This suggests a higher concentration of aluminum in PSA+F, which can be explained by the changes taking place at the surface of PSA during NaF treatment. Initially, the PSA surface is mainly covered by aluminum phosphate (and some sulfates), as indicated by Figure 3a−c. During immersion, fluoride-induced dissolution of surface phosphates is taking place, as seen by the reduced peak intensities of PO_3^- and $AlPO_4^-$ (Figure 3b,c) and concluded by XPS analysis. Consequently, the aluminum (oxide) concentration increases at the surface. In addition, few hydroxyl groups are newly revealed (or created) at the surface. $AlOH^+$ does not reflect the hydroxyl fraction variations and seems to be strongly influenced by the aluminum concentration. One must be cautious with semiquantitative interpretations of ToF-SIMS data, as intensities are dependent not merely on actual concentrations but also on ionization probabilities, which are matrix-dependent. Nevertheless, semiquantitative interpretation is possible if samples have similar chemistries and secondary ion fragments are properly selected.[25] Fragments such as $AlO_3H_2^-$ and $Al_2O_5H_3^-$ (found at nominal masses 77 and 137 m/z (Figure 5d,e) can be considered to be saturated with hydroxyl groups, similar to the 0F fragment in Figure 4a. The intensity distribution of these "hydroxyl saturated" fragments
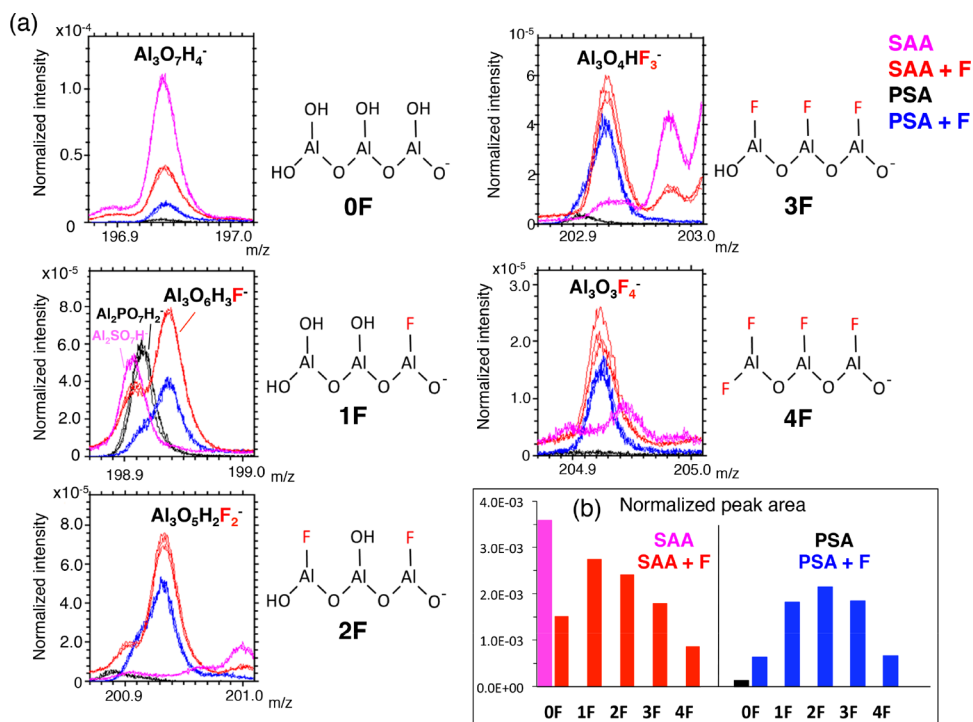
Figure 4. Comparison of the (normalized) ToF-SIMS spectra of higher mass range fragments containing fluorides and hydroxyls, including illustrations of the proposed structures (a), prepared by overlaying three spectra per sample and bar graph showing the intensity distribution of the different fragments among the measured specimens (b).
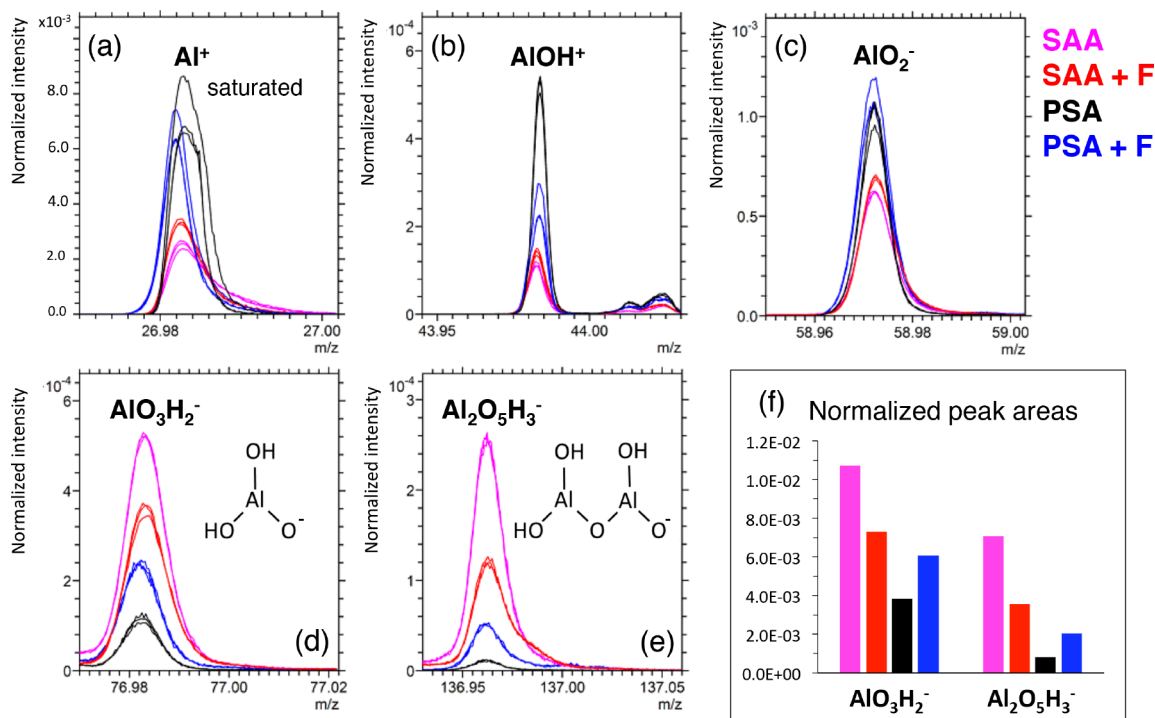
Figure 5. (a−e) Comparison of the (normalized) ToF-SIMS spectra of fragments studied to extract information about the hydroxyl fraction (overlay of three spectra per sample). (f) Bar graph showing the intensity distribution of the average (normalized) peak areas of two saturated OH fragments.

matches quite well with the XPS results. Normalized peak areas are plotted in Figure 5f and support the theory that the hydroxyl fraction of SAA anodized oxides significantly decreases after NaF treatment, while the hydroxyl fraction of PSA anodized oxides increases after NaF treatment. These results illustrate that the chemical modifications taking place

during immersion are dependent on the initial chemical composition.

Morphological Analysis of Porous AAO. The anodizing conditions and the measured morphological features of the porous AAO are listed in Table 3. Figure 6a,b displays the TEM cross-section images from the porous specimens pSAA

Table 3. Anodizing Conditions and Morphological Features As Measured on TEM Cross-Section Images

annotation	H$_2$SO$_4$ (g/L)	H$_3$PO$_4$ (g/L)	anodizing temp (°C)	voltage (V)	oxide thickness (μm)	pore diameter (nm)		barrier layer thickness (nm)
						[top][a]	[bottom][b]	
pSAA[c]	10		50	19	5.0	22	8	17
pSAA + F	25		35	21	5.4	24	10	22
pPSA[c]	50	80	35	19	3.0	28	15	20
pPSA + F	10	40	35	28	4.8	34	28	26

[a]Top = in the vicinity of the oxide/resin interface. [b]Bottom = in the vicinity of the metal/oxide interface. [c]While specimens prepared in exactly the same conditions were not available at the time of TEM observations and analysis, specimens with similar morphological features were selected for morphological comparison. Oxides with these modified anodizing conditions were only used for TEM observations, while panels prepared in the original conditions (with and without fluoride immersion) were applied in floating roller peel tests.
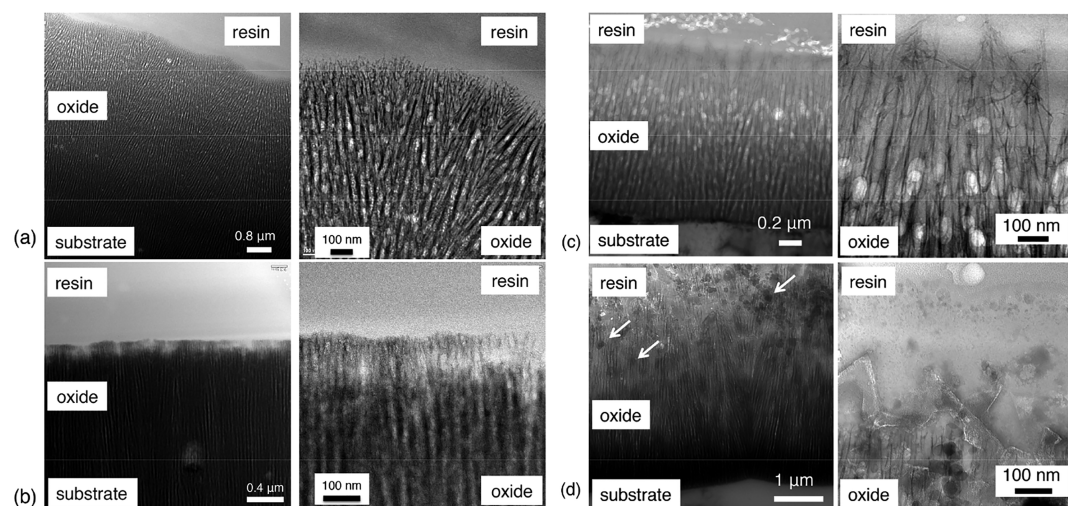
Figure 6. Bright-field TEM cross-section images and a higher magnification image from the oxide/resin interface is shown on the right of (a) pSAA, (b) pSAA+F, (c) pPSA, and (d) pPSA+F. Black spots in image (d), indicated by the arrows, were identified as NaF particles by TEM-EDS analysis. The circular white spots that are especially visible on image (c) are caused by preparation artifacts. Because the TEM lamellas are not prepared exactly vertical to the surface, some of the pores show as circles.

and pSAA+F. Both oxides have comparable thickness, pore diameter, and barrier layer thickness (Table 3). The mere distinction between the two morphologies is evident at the oxide/resin interface. The top of the AAO seems to be reduced in density by the NaF treatment, and the nanosized oxide branches visible at the top of pSAA (Figure 6a) appear to be smoothed out for the pSAA+F sample (Figure 6b). Some dissolution of the porous AAO can be expected by the NaF solution due to the pH = 11.6 as well as the fluorines.

Figure 6 displays the bright-field TEM images of pPSA and pPSA+F (Figure 6c,d, respectively), prepared in the conditions listed in Table 3. In contrast to pSAA morphologies, pPSA oxides are more porous. This is generally associated with the aggressive nature of phosphoric acid, especially when combined with relatively high electrolyte temperatures.[20] This results in an open structure with wider and partially dissolved pores in the vicinity of the oxide/resin interface, often leading to the partial collapse of the surface pore walls, creating a structure that resembles a bird's nest with nano- and microporosity. Consequently, pPSA oxide surface presents a rough interface compared to pSAA (Figure 6c). The differences between pPSA and pPSA+F are also visible at the resin/oxide interface. The general pore structure is similar; however, the very rough features at the top part that were present at pPSA oxide seem to be completely removed by the fluorides in pPSA+F. Fluoride-induced dissolution seems to have almost completely dissolved the upper part of the pPSA oxides, leaving behind an

interface with significantly reduced surface roughness and fine features.

Black spots in Figure 6d can be seen on the oxide, especially at the top part, which obscures some of the morphological features. Plasma cleaning of the thin lamella does not eliminate these features, indicating that they are inherently part of the sample. These were identified by TEM-EDS analysis as NaF particles. It appears that the specimen was not properly rinsed, leaving excess amounts of sodium fluoride in the oxide. Analysis cannot conclusively tell if the presence of NaF in the form of small crystals/particles is inherent to the sample or caused by Ga ion beam induced recrystallization or damage.

X-ray EDS measurements were also performed on the TEM lamellas. Concentration profiles of all the detected elements are presented in Figures S3 and S4 in the Supporting Information for pSAA and pPSA, respectively. The three different phases: aluminum, oxide, and resin are clearly distinguished by their different composition. The oxide mainly consists of aluminum and oxygen, with low amounts of electrolyte-derived anions (2−3 wt % S and ∼1 wt % P in pPSA).[21] In both oxides, fluorine was hardly detected during TEM-EDS profile measurements. Fluorine at very low concentration (≤1.0 wt %) was detected in pSAA+F by point analysis of various carefully chosen areas along the oxide/resin interface. Conversely, fluorine (∼0.2 wt %) was detected on the pPSA+F oxide (especially in the vicinity of the oxide/resin interface). However, sodium was also detected, and this could be due
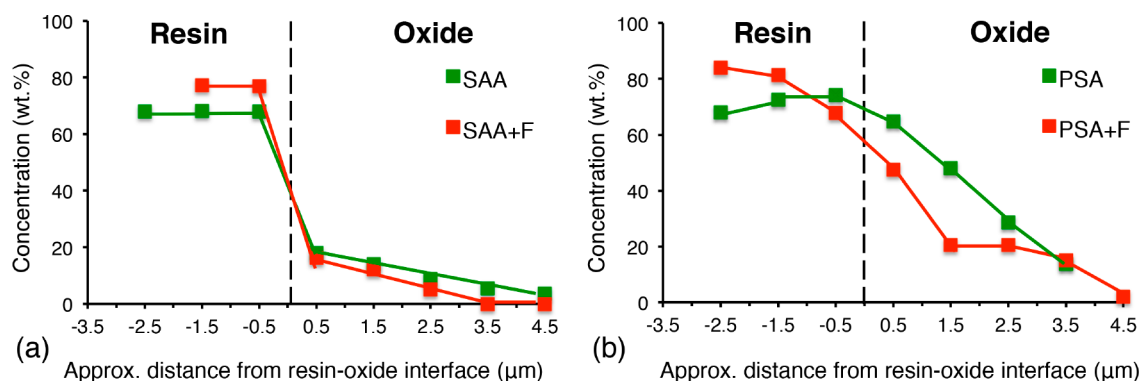
Figure 7. EDS profile showing the carbon concentration across the oxide and resin for (a) pSAA and pSAA+F and (b) pPSA and pPSA+F.
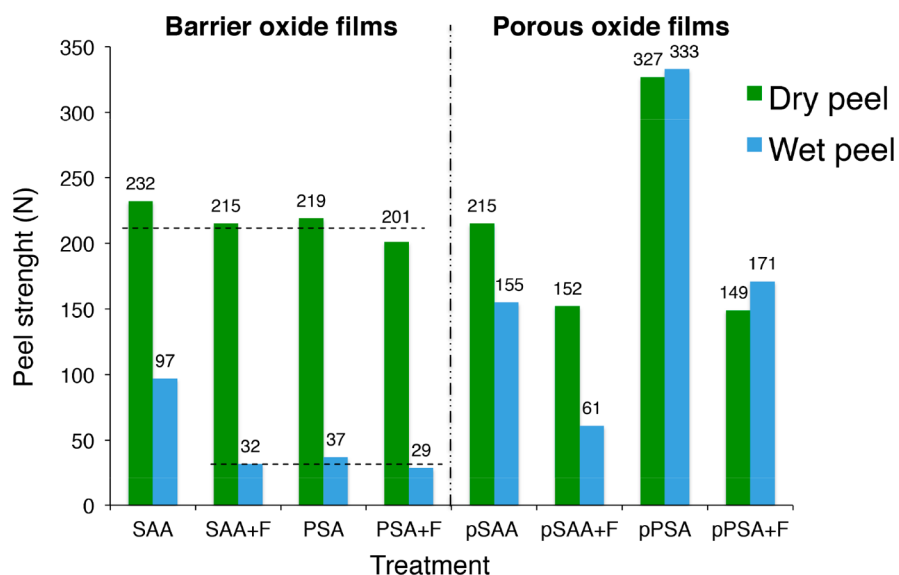

Figure 8. Peel strength before and after NaF dip for barrier AAO (a) SAA, SAA+F and (b) PSA, PSA+F and porous AAO (c) pSAA, pSAA+F and (d) pPSA, pPSA+F. Values are the average measured from six specimens.

to the presence of the NaF contamination (black spots in Figure 6d).

The organic resin is mostly composed of carbon and oxygen. Inorganic additives such as silicon and bromine were also detected in the resin. Approximately 0.1 wt % Si was detected only in the resin, while bromine was detected within the oxide, with an increasing concentration toward the oxide/resin interface and a final concentration of 4−10 wt % within the bulk of the resin. Bromine concentration generally follows the same trend as the carbon profile (Figures S3 and S4 in the Supporting Information), providing a clear indication for the presence of resin inside the pores. Hence, the carbon profiles are further used as an indication for the extent of resin penetration. Comparisons between the carbon concentration profile in pSAA and pSAA+F, as well as pPSA and pPSA+F, are shown in Figure 7a,b, respectively. In both cases, the two different specimens exhibit very similar profiles, indicating that resin penetration was not prohibited by the immersion in NaF and that the so-called mechanical anchoring was not prevented. Generally, carbon profile concentration in pPSA and pPSA+F is more gradual compared to pSAA and pSAA+F, since the pores are larger and the top of the oxide is thinned.

Adhesion Evaluation by Floating Roller Peel Tests.
Adhesion of Barrier AAOs. Following the characterization of

the oxide properties, floating roller peel tests were performed to evaluate the adhesion strength of the oxides bonded with typical aerospace epoxy resins. By measuring the peel strength of bonded panels with barrier-type oxides we minimize the effect of surface roughness, focusing on the role of surface chemistry in interfacial adhesion. These results are plotted in Figure 8, and an image of the panels after testing is shown in Figure S5 in the Supporting Information.

Peel measurements on barrier-type oxides bonded with FM 73 epoxy show that only a minor reduction in dry peel strength is found after fluoride treatments. This is in line with previous research in which adhesion strength is effectively independent of the oxide chemistry, obtained by various anodizing treatment and electrolyte temperatures.[18] Optimum peel strength with cohesive fracture of the adhesive is obtained with an interface strength that is higher than the yield strength of the epoxy adhesive.[26] Apparently dry adhesion is even easy to achieve on a flat, featureless, oxide through dipole−dipole interactions and hydrogen bonding, probably because both Al_2O_3 and primers/adhesives are polar. In spite of the fact that fluorides can reduce the surface energy,[27−29] a few percent of fluorine on the AAO surface do not cause dramatic reduction in their dry peel strength.

Under wet conditions, however, there is a threefold loss of peel strength in SAA+F compared to SAA, while the

performance of PSA+F remains similar to that of PSA. These results are in excellent agreement with our earlier findings, which show that the wet peel strength of barrier-type oxides is proportional to the amount of surface hydroxyls.[18] The same trend is observed here; SAA with the largest amount of hydroxyls in this group (OH ≈ 23%, Table 1) exhibiting the highest wet peel strength, while all the other oxides (SAA +F, PAS, and PSA+F) exhibit similar performance, as they contain a similar amount of surface hydroxyls (OH ≈ 15%, Table 1). Because some phosphates that were present on the surface of PSA were dissolved to reveal new surface hydroxyls on PSA+F, as measured by XPS and ToF-SIMS, the net effect of fluoride on the surface chemistry of PSA+F is small. As a consequence, there is no significant change in bond strength under wet conditions, and no further adhesion loss is registered.

It is well-established that interfacial bonding largely depends on the chemical affinities between the surface and the resin. Hence, chemical modifications to the oxide play important role in determining the type and strength of interfacial bonding.[30,31] Studies on surface fluorination have shown that replacement of surface H, OH⁻, and O^{2-} sites by fluorides alter the surface properties significantly,[27−29,32,33] but with the few percent fluorine on the AAO surface in this study, no dramatic reduction in wet peel strength is found. As a consequence, the relation between OH% and wet peel strength that was previously found on barrier-type oxides still remains after fluorine treatment (Figure S7a).

Adhesion of Porous AAOs. Since industrially applied AAOs are porous, their interfacial adhesion is affected by changes in the surface chemistry, as well as changes in the morphology, including differences in the surface roughness. Therefore, their adhesion performance will be affected by changes in both parameters. Peel test results for porous oxides are displayed in Figure 8 for pSAA and pPSA, respectively. In all cases there is a significant reduction in the bond strength after fluoride treatments, under both dry and wet conditions. Compared to pSAA, dry peel strength after fluoride treatment (pSAA+F) is reduced by 30% (from 215 to 152 N), while the wet peel strength is reduced by 60% (from 155 to 61 N). As the dry peel of barrier AAO was not significantly affected by changes in the surface chemistry due to fluoride treatment, the initial 30% reduction in dry conditions is rather unexpected. In our previous research on porous AAOs practically all the studied anodizing pretreatments resulted in good dry adhesion, unless the pores were too small for the primer to fully penetrate and fill the pores.[18−20] When pores are not properly filled, it results in a lower contact surface for bonding, and the negative impact of these unfilled cavities is effective at dry peel as well as wet peel strength. Although both surface chemistry and oxide morphology were affected by the NaF immersion, as shown by TEM images, still a proper filling of the pores was confirmed with the carbon profile measured by TEM-EDS. Hence, the dry peel strength of the porous AAOs after fluoride immersion appears to deviate from this general trend, as shown in Figure S6a in the Supporting Information. In the absence of extended surface roughness, it is most likely that the surface chemistry of the porous oxides after NaF immersion will play a more significant role than for barrier oxides. Replacing hydroxides with fluorine can lead to a reduction in the surface energy[27−29] and negatively affect depletion/wetting between the primer and the porous oxide.[34] Consequently, the attractive interface forces as created by surface hydroxides, such as

dipole−dipole and hydrogen bonding, are replaced by much weaker van der Waals forces due to the presence of the fluorides. These much weaker interfacial bonds require an extremely high surface area to collectively play a decisive role in interfacial interactions, as in the famous Gecko example and its man-made imitations,[35−39] a parameter that is clearly missing after fluorides-induced dissolution of the fine features at the top surface of the pores. Additionally, the difference in adhesion could be explained by the use of a phenol-formaldehyde primer with the porous oxides, compared with an epoxy adhesive that was used with the barrier oxides. A phenol-formaldehyde is expected to give less adhesion than an epoxy, a parameter that previously did not play a significant role in dry porous oxides with rough interface.[18−21] Furthermore, there can also be a geometric effect, since load transfer between adhesive and porous anodic oxide is primarily by shear at pore surfaces. While usually the shear strength of an interface is lower than the tensile normal strength,[26] as applicable with featureless barrier type oxides, any of the above adhesion reductions will consequently be more effective on porous oxides. Further research is needed to identify the dominant cause of this reduction.

Under wet conditions, we expect to measure a reduction in the peel strength of the porous oxide pSAA+F due to partial replacement of surface hydroxyls by fluorides, as established for the barrier oxide SAA+F. Indeed, the relative wet peel strength reduction from 155 to 61 N for pSAA versus pSAA+F is in agreement with the relative wet peel strength reduction from 97 to 33 N for SAA versus SAA+F. This implies that, for both SAA oxide types, the wet peel strength is dominated by surface hydroxides, and similar quantitative adhesion loss can be explained by the partial replacement of surface hydroxides by fluorides.

When we previously compared the peel strength of porous AAOs in dry conditions with wet conditions,[20] it was observed that properly filled oxide pores with sufficient dry adhesion have failed in wet conditions when produced by less than optimal anodizing parameters (chemicals and electrolyte temperature) that produced low nano- and microsurface roughness.[20] While with barrier-type oxides a poor wet adhesion is obtained with PSA due to relatively low OH concentrations, typically with porous oxides higher wet peel strengths are obtained with PSA than with SAA. This difference can be explained either by possible differences in surface chemistry between barrier oxides and porous oxides or by the high surface area with nanofibrils created by PSA. Typically with barrier oxides practically no oxide dissolution has occurred within the 4−8 s of pretreatment, while with porous oxides a substantial part of the surface has been dissolved with PSA due to the presence of phosphoric acid in the anodizing electrolyte, as shown by van Put et al.[40] While with pSAA a reasonable amount of surface hydroxyls is formed by anodizing, still an increase strength can be obtained in moisture-resistant adhesion by immersion in H_3PO_4 solution, as shown by Yendall et al.[41] Considering the good wet peel values obtained with phosphoric sulfuric acid anodizing (as well as high-temperature sulfuric acid anodizing[11]), the oxide dissolution does not only affect the surface morphology but may also yield an increased concentration of surface hydroxyls. Therefore, pPSA oxides typically deliver excellent peel strength in both dry and wet conditions. After NaF treatment, however, both dry and wet peel strengths of pPSA+F are significantly reduced. The surprising reduction of dry adhesion is contributed to an

interplay between surface-energy changes affecting the type of attractive forces across the interface, as well as the loss of fine surface features, as seen by TEM cross-section images, as was also described with pSAA+F. The slight difference in wet environment compared to dry conditions is negligible (49% and 55%, respectively). Since chemical analysis shows that the net effect of fluorine adsorption on the surface chemistry of PSA+F is small, we do not expect adhesion reduction of its porous equivalent to be occurring due to OH loss, as in pSAA+F. More likely, both peel strength values are dominated by the reduced surface polarity and effective surface area after NaF immersion. The relative adhesion loss on pPSA+F compared to pSAA+F in wet conditions (∼50%), confirms this hypothesis. The somewhat reduced effect with pPSA+F can be explained by the replacement of surface phosphates by new OH groups.

CONCLUSIONS

The mechanism of surface chemical modification caused by NaF post-treatment immersion was clarified by XPS and ToF-SIMS chemical analysis of barrier-type AAOs. Measurements reveal not only that surface hydroxyls are partially replaced by fluorides but also that the impact on oxide composition depends on the initial surface chemistry. While the amount of surface hydroxyls on SAA+F is significantly reduced due to fluorides adsorption, dissolution of surface phosphates in PSA+F (which previously dominated the PSA surface composition) reveals new OH groups that compensate for fluorine adsorption, and therefore, the net OH fraction remains similar (and even somewhat increases). Morphological modifications, as reveled by TEM images, show that NaF immersion caused dissolution of the nanofibrils at the top AAO surface. However, carbon concentration profiles measured by TEM-EDS are similar to the ones before NaF immersion, indicating that primer is still able to fill the pores.

On the one hand, in spite of the fact that fluorides can reduce the surface energy, a few percent of fluorine on the AAO surface do not cause dramatic reduction in dry adhesion of flat, featureless AAOs, probably because both Al_2O_3 and primers/adhesives are polar. Reduced dry adhesion, on the other hand, is measured on the porous equivalent. This adhesion loss is probably caused by interplay of multiple parameters, including: surface energy changes affecting the type of attractive forces across the interface, as well as the loss of fine surface features that contribute to an extended surface area and (nano-) roughness. Further research is needed to identify the dominant cause.

It is more difficult to obtain water-resistant adhesion in which the number of OH groups is of great importance for stable bonding, even for a partially fluorinated AAO surface. By replacing water-stable OH surface interaction sites with fluorides, a significant loss of bond strength of SAA+F is measured under water ingress for both barrier and porous oxides.

This study expands our knowledge on the different mechanisms that contribute to adhesion of AAOs and, for the first time, unambiguously distinguish contributions from interfacial chemistry in porous AAOs. The results demonstrate a clear relation between interfacial modifications on the nanoscale and macroscopic interface strength. Hereby we hope to encourage further research on similar systems of industrial relevance, as a better fundamental understanding can lead to further improvements of durable adhesion.

ASSOCIATED CONTENT

Ⓢ Supporting Information

The Supporting Information is available free of charge on the ACS Publications website at DOI: 10.1021/acsanm.8b01361.

Supplementary figures, including Eh−pH diagrams for F−Al−H$_2$O and Al−F−H$_2$O systems, concentration profiles obtained by EDS for all the elements measured on TEM cross sections that are shown in Figure 6, images of barrier AAOs specimens after floating roller peel tests and a comparison between the peel strength measured in this study to the general trends of that were discussed in the previous paper[20] (PDF)

AUTHOR INFORMATION

Corresponding Author
*E-mail: Herman.Terryn@vub.be.

ORCID
J. M. C. Mol: 0000-0003-1810-5145
H. Terryn: 0000-0003-2639-5496

Notes
The authors declare no competing financial interest.

REFERENCES

(1) Runge, J. M. *The Metallurgy of Anodizing Aluminum*; Springer, 2018.

(2) Lee, W.; Park, S.-J. Porous Anodic Aluminum Oxide: Anodization and Templated Synthesis of Functional Nanostructures. *Chem. Rev.* **2014**, *114*, 7487−7556.

(3) Ali, H. O. Review of Porous Anodic Aluminium Oxide (Aao) Applications for Sensors, Mems and Biomedical Devices. *Trans. Inst. Met. Finish.* **2017**, *95*, 290−296.

(4) Losic, D.; Lillo, M.; Losic, D. Porous Alumina with Shaped Pore Geometries and Complex Pore Architectures Fabricated by Cyclic Anodization. *Small* **2009**, *5*, 1392.

(5) Critchlow, G. W.; Brewis, D. M. Review of Surface Pretreatments for Aluminium Alloys. *Int. J. Adhes. Adhes.* **1996**, *16*, 255−275.

(6) Zhou, X.; Liu, Y.; Thompson, G. E.; Scamans, G. M.; Skeldon, P.; Hunter, J. A. Near-Surface Deformed Layers on Rolled Aluminum Alloys. *Metall. Mater. Trans. A* **2011**, *42*, 1373−1385.

(7) Abrahami, S. T.; de Kok, J. M. M.; Terryn, H.; Mol, J. M. C. Towards Cr(Vi)-Free Anodization of Aluminum Alloys for Aerospace Adhesive Bonding Applications: A Review. *Front. Chem. Sci. Eng.* **2017**, *11*, 1−18.

(8) Lunder, O.; Simensen, C.; Yu, Y.; Nisancioglu, K. Formation and Characterisation of Ti−Zr Based Conversion Layers on Aa6060 Aluminium. *Surf. Coat. Technol.* **2004**, *184*, 278−290.

(9) Våland, T.; Nilsson, G. The Influence of F− Ions on the Electrochemical Reactions on Oxide-Covered Al. *Corros. Sci.* **1977**, *17*, 449−459.

(10) Furrer, G.; Stumm, W. The Coordination Chemistry of Weathering: I. Dissolution Kinetics of Δ-Al2o3 and Beo. *Geochim. Cosmochim. Acta* **1986**, *50*, 1847−1860.

(11) Cerezo, J.; Taheri, P.; Vandendael, I.; Posner, R.; Lill, K.; de Wit, J. H. W.; Mol, J. M. C.; Terryn, H. Influence of Surface Hydroxyls on the Formation of Zr-Based Conversion Coatings on Aa6014 Aluminum Alloy. *Surf. Coat. Technol.* **2014**, *254*, 277−283.

(12) Jagminas, A.; Vrublevsky, I.; Kuzmarskytė, J.; Jasulaitienė, V. Composition, Structure and Electrical Properties of Alumina Barrier Layers Grown in Fluoride-Containing Oxalic Acid Solutions. *Acta Mater.* **2008**, *56*, 1390−1398.

(13) Elaish, R.; Curioni, M.; Gowers, K.; Kasuga, A.; Habazaki, H.; Hashimoto, T.; Skeldon, P. Effect of Fluorozirconic Acid on Anodizing of Aluminium and Aa 2024-T3 Alloy in Sulphuric and Tartaric-Sulphuric Acids. *Surf. Coat. Technol.* **2018**, *342*, 233–243.

(14) Jagminas, A.; Kuzmarskytè, J.; Malferrari, L.; Cuffiani, M. A New Route of Alumina Template Modification into Dense-Packed Fibrilous Material. *Mater. Lett.* **2007**, *61*, 2896–2899.

(15) Yaniv, A. E.; Klein, I. E. Anodizing in Fluoroboric Acid Solution. *Corros. Sci.* **1971**, *11*, 343–IN3.

(16) Elaish, R.; Curioni, M.; Gowers, K.; Kasuga, A.; Habazaki, H.; Hashimoto, T.; Skeldon, P. Effects of Fluoride Ions in the Growth of Barrier-Type Films on Aluminium. *Electrochim. Acta* **2017**, *245*, 854–862.

(17) Venables, J. D.; McNamara, D. K.; Chen, J. M.; Sun, T. S.; Hopping, R. L. Oxide Morphologies on Aluminum Prepared for Adhesive Bonding. *Appl. Surf. Sci.* **1979**, *3*, 88–98.

(18) Abrahami, S. T.; Hauffman, T.; de Kok, J. M. M.; Mol, J. M. C.; Terryn, H. Effect of Anodic Aluminum Oxide Chemistry on Adhesive Bonding of Epoxy. *J. Phys. Chem. C* **2016**, *120*, 19670–19677.

(19) Abrahami, S.; Hauffman, T.; de Kok, J. M. M.; Terryn, H.; Mol, A. Adhesive Bonding and Corrosion Performance Investigated as a Function of Aluminum Oxide Chemistry and Adhesives. *Corrosion* **2017**, *73*, 903–914.

(20) Abrahami, S. T.; de Kok, J. M. M.; Gudla, V. C.; Ambat, R.; Terryn, H.; Mol, J. M. C. Interface Strength and Degradation of Adhesively Bonded Porous Aluminum Oxides. *NPJ. Mater. Degrad.* **2017**, *1*, 8.

(21) Abrahami, S. T.; Hauffman, T.; de Kok, J. M. M.; Mol, J. M. C.; Terryn, H. Xps Analysis of the Surface Chemistry and Interfacial Bonding of Barrier-Type Cr(Vi)-Free Anodic Oxides. *J. Phys. Chem. C* **2015**, *119*, 19967–19975.

(22) Sheasby, P. G.; Pinner, R. *Surface Treatment and Finishing of Aluminium and Its Alloys,* 6th ed.; Finishing Publications Ltd.: England, 2001.

(23) *Standard Test Method for Floating Roller Peel Resistance of Adhesives,* D3167-03a; ASTM International: West Conshohocken, PA, 2003.

(24) Kemnitz, E.; Kohne, A.; Grohmann, I.; Lippitz, A.; Unger, W. E. S. X-Ray Photoelectron and X-Ray Excited Auger Electron Spectroscopic Analysis of Surface Modifications of Chromia During Heterogeneous Catalyzed Chlorine/Fluorine Exchange. *J. Catal.* **1996**, *159*, 270–279.

(25) Vickerman, J. C.; Gilmore, I. S. *Surface Analysis—the Principal Techniques;* John Wiley & Sons, Ltd, 2009; pp 653–666.

(26) de Kok, J. M. M.; Peijs, T. Deformation, Yield and Fracture of Unidirectional Composites in Transverse Loading: 2. Influence of Fibre–Matrix Adhesion. *Composites, Part A* **1999**, *30*, 917–932.

(27) Hayes, L. J. Surface Energy of Fluorinated Surfaces. *J. Fluorine Chem.* **1976**, *8*, 69–88.

(28) Jarvis, N. I.; Zisman, W. A. *Surface Chemistry of Fluorochemicals,* Report 6324; U.S. Naval Research Laboratory: Washington D.C., 1965.

(29) du Toit, F. J.; Sanderson, R. D.; Engelbrecht, W. J.; Wagener, J. B. The Effect of Surface Fluorination on the Wettability of High Density Polyethylene. *J. Fluorine Chem.* **1995**, *74*, 43–48.

(30) Petersen, J.; Fouquet, T.; Michel, M.; Toniazzo, V.; Dinia, A.; Ruch, D.; Bomfim, J. A. S. Enhanced Adhesion over Aluminum Solid Substrates by Controlled Atmospheric Plasma Deposition of Amine-Rich Primers. *ACS Appl. Mater. Interfaces* **2012**, *4*, 1072–1079.

(31) Mosebach, B.; Ozkaya, B.; Giner, I.; Keller, A.; Grundmeier, G. Analysis of Acid-Base Interactions at Al2o3 (11−20) Interfaces by Means of Single Molecule Force Spectroscopy. *Appl. Surf. Sci.* **2017**, *420*, 296–302.

(32) Hess, A.; Kemnitz, E.; Lippitz, A.; Unger, W. E. S.; Menz, D. H. Esca, Xrd, and Ir Characterization of Aluminum Oxide, Hydroxyfluoride, and Fluoride Surfaces in Correlation with Their Catalytic Activity in Heterogeneous Halogen Exchange Reactions. *J. Catal.* **1994**, *148*, 270–280.

(33) Hess, A.; Kemnitz, E. Characterization of Catalytically Active Sites on Aluminum Oxides, Hydroxyfluorides, and Fluorides in Correlation with Their Catalytic Behavior. *J. Catal.* **1994**, *149*, 449–457.

(34) Denesuk, M.; Zelinski, B. J. J.; Kreidl, N. J.; Uhlmann, D. R. Dynamics of Incomplete Wetting on Porous Materials. *J. Colloid Interface Sci.* **1994**, *168*, 142–151.

(35) Autumn, K.; Peattie, A. M. Mechanisms of Adhesion in Geckos1. *Integr. Comp. Biol.* **2002**, *42*, 1081–1090.

(36) Autumn, K.; Sitti, M.; Liang, Y. A.; Peattie, A. M.; Hansen, W. R.; Sponberg, S.; Kenny, T. W.; Fearing, R.; Israelachvili, J. N.; Full, R. J. Evidence for Van Der Waals Adhesion in Gecko Setae. *Proc. Natl. Acad. Sci. U. S. A.* **2002**, *99*, 12252–12256.

(37) Gong, G.; Zhou, C.; Wu, J.; Jin, X.; Jiang, L. Nanofibrous Adhesion: The Twin of Gecko Adhesion. *ACS Nano* **2015**, *9*, 3721–3727.

(38) Murphy, M. P.; Kim, S.; Sitti, M. Enhanced Adhesion by Gecko-Inspired Hierarchical Fibrillar Adhesives. *ACS Appl. Mater. Interfaces* **2009**, *1*, 849–855.

(39) Wang, Z. Slanted Functional Gradient Micropillars for Optimal Bioinspired Dry Adhesion. *ACS Nano* **2018**, *12*, 1273.

(40) van Put, M.; Abrahami, S. T.; Elisseeva, O.; de Kok, J. M. M.; Mol, J. M. C.; Terryn, H. Potentiodynamic Anodizing of Aluminum Alloys in Cr(Vi)-Free Electrolytes. *Surf. Interface Anal.* **2016**, *48*, 946–952.

(41) Yendall, K. A.; Critchlow, G. W. Novel Methods, Incorporating Pre- and Post-Anodising Steps, for the Replacement of the Bengough–Stuart Chromic Acid Anodising Process in Structural Bonding Applications. *Int. J. Adhes. Adhes.* **2009**, *29*, 503–508.